Near-infrared spectroscopy of H_3^+ above the barrier to linearity

Jennifer L. Gottfried,[a] Benjamin J. McCall,[b] and Takeshi Oka
Department of Chemistry, Department of Astronomy & Astrophysics, the Enrico Fermi Institute,
University of Chicago, Chicago, Illinois 60637

The first H_3^+ transitions above the barrier to linearity have been observed in absorption in the near infrared using a highly sensitive dual-beam, double-modulation technique with bidirectional optical multipassing. A total of 22 rovibrational transitions of H_3^+ have been detected and assigned to the fourth and fifth overtone and combination bands ($5\nu_2^1$, $5\nu_2^5$, $2\nu_1+2\nu_2^2$, $3\nu_1+\nu_2^1$, $\nu_1+4\nu_2^2$, $2\nu_1+3\nu_2^1$, and $6\nu_2^2$). These transitions, which are more than 4600 times weaker than the fundamental band, probe energy levels above $10\,000$ cm^{-1}, the regime in which H_3^+ has enough energy to sample linear configurations. Experimentally determined energy levels above the barrier to linearity provide a critical test of *ab initio* calculations in this challenging regime. The comparison between experimental energy levels and theoretical energy levels from *ab initio* calculations in which the adiabatic and relativistic corrections are incorporated reveals the extent of higher-order effects such as nonadiabatic and radiative corrections. We compare our results with several recent theoretical calculations. © *2003 American Institute of Physics.* [DOI: 10.1063/1.1575737]

I. INTRODUCTION

The molecular ion H_3^+, the simplest stable polyatomic molecule, performs an important role in the chemistry of hydrogen-rich plasmas and in the evaluation of theoretical calculations of rovibrational levels in polyatomic molecules. The ground-state equilibrium geometry of H_3^+ is an equilateral triangle, resulting in unusual spectroscopic properties. An obvious consequence of this high degree of symmetry is that the ion has no permanent dipole moment and, thus, no ordinary rotational spectrum. No stable electronic excited states of H_3^+ have ever been observed, and in fact theory suggests that a discrete electronic spectrum is unlikely to exist. The only available spectroscopic signature of H_3^+, therefore, is its vibrational spectrum.

The initial motivation for the laboratory spectroscopy of H_3^+ was to facilitate its astronomical study. As the most abundantly produced molecular ion in interstellar clouds, H_3^+, the universal proton donor, plays the most fundamental role in the chemistry of the interstellar medium. The infrared absorption spectrum of H_3^+ was first observed in the laboratory by Oka in 1980.[1] Trafton *et al.*[2] made the first nonterrestrial observation of H_3^+ in the ionosphere of Jupiter in 1987, although it was not positively identified until 1989.[3] More recently, H_3^+ has been detected in the interstellar medium.[4,5] Since then, many additional H_3^+ spectra have been recorded, both in the laboratory and in space—and H_3^+ has been the focus of many reviews.[6–15] With numerous theoretical studies and 17 laboratory spectroscopic studies including over 800 observed transitions, the spectrum of H_3^+ below 9000 cm^{-1} is well understood.[14]

Collaborative effort between experimentalists and theo-

rists has been essential in the development of H_3^+ spectroscopy: theoretical predictions help the experimentalists' search for new transitions, and accurate experimental frequencies enable theorists to improve the potential energy surfaces and variational calculations. In this paper, we present the results of a new laboratory investigation of overtone and combination bands of H_3^+, beyond the barrier to linearity and higher in energy than any previously detected transitions. These transitions, which are more than 4600 times weaker than the fundamental band,[16] occur in the near-infrared region and were observed in absorption. The detection of these transitions required the development of a high-resolution, high-sensitivity spectrometer.

An experimental setup using the combined techniques of velocity modulation (VM), phase modulation (PM) with heterodyne detection, bidirectional optical multipassing, and dual-beam subtraction was developed in order to detect these extremely weak H_3^+ transitions. The velocity modulation,[17] which is commonly used in positive column plasma spectroscopy to modulate and discriminate ion lines from neutral lines, is supplemented by phase modulation and heterodyne detection[18] at 500 MHz to minimize the $1/f$ noise of the laser. The overall sensitivity is close to shot-noise limited, as detailed in Sec. III.

The primary motivation for continuing the study of vibrational states beyond those spectroscopically probed to date is to assist in the development of theoretical calculations of H_3^+. The variational treatment of the kinetics of three protons in the *ab initio* potential surfaces, which has been successful so far, may not be as effective near the barrier to linearity due to a singularity in the Hamiltonian that occurs whenever H_3^+ samples a linear configuration. Experimentally determined energy levels are therefore essential as a check for various theoretical techniques for calculating the energy levels to spectroscopic accuracy and studying higher-order

[a]Electronic mail: jgottfri@uchicago.edu
[b]Present address: Department of Chemistry and Department of Astronomy, University of California at Berkeley, Berkeley, CA 94720-3411.

effects such as the adiabatic and nonadiabatic corrections to the Born–Oppenheimer approximation, as well as relativistic and radiative corrections. Although the high-energy levels $(>11\,000 \text{ cm}^{-1})$ in this work are considerably above the highest levels observed thus far in the astronomical plasmas of Jupiter's ionosphere (6669 cm^{-1} in the overtone band[3] and 7992 cm^{-1} in hot bands[19]), they may be observable in Jupiter and other high-temperature astronomical objects in the near future.

II. BACKGROUND

A. Quantum numbers

As a symmetric top molecule with D_{3h} symmetry, H_3^+ has three vibrational degrees of freedom resulting in two modes: the totally symmetric (A_1') mode ν_1 is infrared inactive, and the doubly degenerate (E') bending mode ν_2 is active. Vibrational states are labeled as $v_1\nu_1 + v_2\nu_2^\ell$, where v_1 and v_2 are the vibrational quantum numbers of the ν_1 and ν_2 modes, and $\ell = v_2, v_2 - 2, \ldots, -v_2$ is the quantum number for vibrational angular momentum.

Because of the small mass of its nuclei and its relatively shallow potential, H_3^+ is a highly anharmonic vibrator and the harmonic selection rules ($\Delta v_2 = 1$ and $\Delta \ell = \pm 1$) are not obeyed, especially for the highly excited states reported in this paper. The quantum number k for the projection of the rotational angular momentum J along the symmetry axis identifies the parity of the level,[20] but is not a convenient quantum number to specify energy and permutation symmetry in excited states of the ν_2 mode, due to the strong Coriolis coupling between the rotational and vibrational angular momentum. Instead, Hougen's quantum number[21] $g = k - \ell$ or its absolute value $G = |k - \ell|$ specifies the energy and symmetry of the rovibrational levels. The quantum number g is associated with the spin modification of H_3^+; $g = 3n$ (n is an integer) corresponds to $ortho$-H_3^+ ($I = 3/2$) and $g = 3n \pm 1$ corresponds to $para$-H_3^+ ($I = 1/2$), where I is the quantum number for the total nuclear spin angular momentum $\hat{I} = \hat{I}_1 + \hat{I}_2 + \hat{I}_3$. The electric dipole selection rules for these quantum numbers are $\Delta g = 3n$ and $\Delta k = odd$, the latter from the selection rule for parity $(-1)^k$. Although the only rigorously good quantum numbers are the quantum number F for the total angular momentum $\hat{F} = \hat{J} + \hat{I}$ and parity $\pm$ (selection rule: $+ \leftrightarrow -$), J and I can be considered good quantum numbers because of the weakness of the nuclear spin–rotation interaction and the selection rules $\Delta I = 0$ and $\Delta J = 0, \pm 1$ are strongly obeyed. The notation used in this paper for H_3^+ transitions is that detailed in the recent review by Lindsay and McCall[14] for both the band symbol

$$v_1\nu_1 + v_2\nu_2^{|\ell|} \leftarrow 0 \qquad (1)$$

and the branch symbol

$$^{\{n|t|\pm 6|\pm 9|\cdots\}}\{P|Q|R\}(J'', G'')^{\{u|l\}}, \qquad (2)$$

where P, Q, and R represent $\Delta J = -1, 0$, and $+1$; u and l differentiate pairs of levels with the same value of G (and different values of k and ℓ) for the upper state. When $\Delta G \neq 0$, the value of ΔG is specified by the leading superscript, where t corresponds to $\Delta G = +3$ and n corresponds to ΔG

$= -3$. For transitions $g' = \pm 2 \leftarrow g'' = -(\pm 1)$, etc., which formally look like $\Delta G = 1$, n is used. For highly mixed levels where g changes by more than 3, the numerical value of ΔG is used ($\pm 6, \pm 9, \ldots$). A more thorough discussion of the quantum numbers and selection rules for H_3^+ can be found in the review by Lindsay and McCall.[14]

B. Theoretical calculations

Because H_3^+ is the simplest polyatomic molecule, a great many $ab\ initio$ theoretical papers have been published on it[14,22] since the earliest work by Coulson[23] in 1935. Just as molecular hydrogen has served as the model for the $ab\ initio$ studies of diatomic molecules, H_3^+ has been used as a benchmark for theoretical calculation of polyatomic molecules from first principles.

Using an $ab\ initio$ potential energy surface,[24] Carney and Porter were the first to calculate rovibrational energies of H_3^+ in 1976.[25] This theoretical prediction helped the laboratory detection[1] of the fundamental band of H_3^+ and its analysis by Watson. The accuracy of $ab\ initio$ calculations improved greatly after the laboratory detection. In 1986, Meyer, Botschwina, and Burton[26] (MBB) published a potential, which, after a small correction by a scaling factor to match the observed ν_2 band origin of H_3^+, gave accurate values and predictions for excited vibrational states of H_3^+ and its isotopomers. The corrected MBB potential has been used extensively by Miller and Tennyson[27–29] for a generation of H_3^+ calculations based on the variational formalism of Sutcliffe and Tennyson.[30] Those calculations were essential for the assignment of the laboratory spectrum of hot bands,[31] overtone bands,[32] and forbidden transitions[33] and the astronomical spectrum of Jupiter.[3] Dinelli, Miller, and Tennyson[34] also used the $ab\ initio$ potential energy surface published by Lie and Frye[35] to generate a spectroscopically determined potential surface.

In the last decade, theoretical calculations have been further improved, reaching near spectroscopic accuracy. Watson[36,37] developed a semiempirical potential energy surface by adjusting the MBB potential to match the laboratory spectrum and provided accurate predictions,[38] which we have used over many years.[14] Röhse, Kutzelnigg, Jaquet, and Klopper[39] (RKJK) published a potential energy surface with microhartree accuracy (errors less than 1 cm^{-1}) in 1994. Dinelli, Polyansky, and Tennyson[40] developed a semiempirical potential based on the RKJK potential which led to the very extensive calculation of Neale, Miller, and Tennyson[41] (NMT), who gave frequencies and intensities for 3 million transitions with high accuracy. The adiabatic correction for the breakdown of the Born–Oppenheimer approximation was calculated by Dinelli $et\ al.$[42] The most accurate potential to date is that of Cencek, Rychlewksi, Jaquet, and Kutzelnigg[43] (CRJK), who took into account adiabatic and relativistic corrections. The most recent calculations based on the CRJK potential have given theoretical values of spectroscopic accuracy.[44–49] Quite independently, Aguado $et\ al.$[50] published a global potential surface which is suitable for dynamical calculations. A recent paper by Lindsay and McCall[14] summarizes the different theoretical approaches
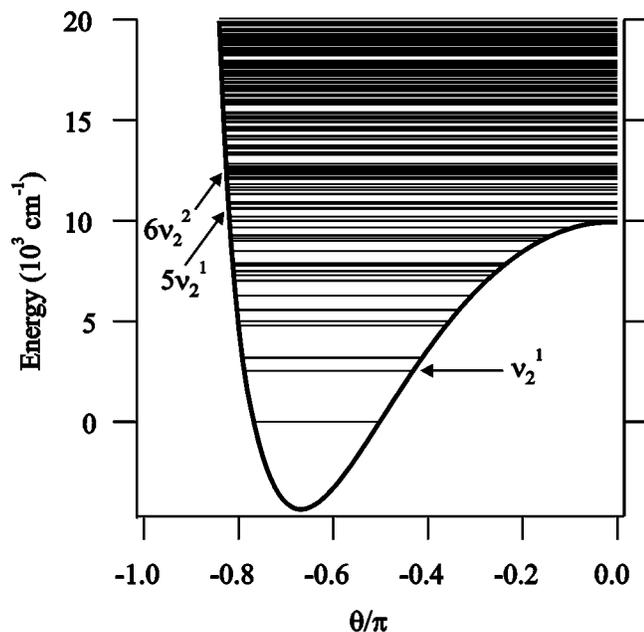
FIG. 1. One-dimensional cut of the potential energy surface of Röhse *et al.* (Ref. 39) along with calculated rotationless ($J=0$) energy levels. This slice of the potential surface was created by varying two equal H–H bond lengths of the H_3^+ molecule to minimize the energy for each value of the angle θ, which measures the deviation from linearity (where $\theta=0$ is the top of the barrier to linearity). The $5\nu_2^1$ and $6\nu_2^2$ levels are completely above the barrier to linearity.

and their agreement with experimental values below the energy of 9000 cm^{-1}.

The energy regime near and above the barrier to linearity is particularly difficult theoretically—until recently, few of the rovibrational calculations performed in this range included the correct boundary conditions for linear geometries. The variational treatment, which is essential in calculating high rovibrational energy levels of H_3^+, encounters a difficulty near the top of the barrier to linearity at the energy of $\sim10\,000$ cm^{-1} above the zero-point level. This is because the kinetic Hamiltonian, which is inversely proportional to the moment of inertia, contains a singularity for the linear structure. Figure 1 shows a one-dimensional cut of the potential energy surface of Röhse *et al.*[39] in which H_3^+ is constrained in an isosceles triangle structure and the two equal H–H bond lengths are varied to minimize the energy for each value of the angle θ, which measures the deviation from linearity. The top of the barrier to linearity is at $\theta=0$ in this figure.

Watson,[36] who used the Morse coordinate system with three H–H bond lengths (r_1, r_2, r_3), confined the wave functions to vanishingly small amplitudes at linear geometries by introducing an artificial wall of 10^6 cm^{-1} for linear ($r_1+r_2=r_3$) and nonphysical ($r_1+r_2<r_3$) regions. While this gave accurate results for levels with energy less than 9000 cm^{-1}, Watson did not expect the calculations to be accurate for higher energy levels and advocated the use of hyperspherical coordinates.[37]

Neale, Miller, and Tennyson[41] used the Jacobi coordinates (r_1, r_2, θ), for which the Hamiltonian has a serious singularity for $r_2=0$. Since the analytical solution of the

Morse potential ($\infty>r>-\infty$) does not satisfy the boundary condition ($\infty>r_2\geqslant0$), they used a basis set composed of spherical oscillator functions. This has allowed them to handle the singularity problem at linear geometries ($\theta=0, \pi$, or $r_2=0$), although a subsequent comparison with experimental energy levels[14] has shown that this method suffers from poor agreement at high rotational levels ($J>8$). This shortcoming has been overcome recently by the use of the Radau coordinates (R_1, R_2, θ), in which the z axis is perpendicular to the plane of the molecule.[51]

A more efficient and elegant way to treat the large amplitude motion of H_3^+ is to use hyperspherical coordinates (ρ, θ, ϕ). The basis set of hyperspherical harmonics not only allows rigorous treatment of singularities in the kinetic Hamiltonian, but also retains the D_{3h} permutation-inversion symmetry of the system, so that full advantage of the symmetry properties of the molecule may be taken. Although Whitnell and Light[52] used hyperspherical coordinates in which the z axis is in the plane of H_3^+ for their calculation of vibrational energy levels ($J=0$), subsequent rovibrational calculations used Johnson's Hamiltonian,[53] which was based on the formulation of Smith and Whitten[54,55] in which the z axis is along the axis of the symmetric top rotor perpendicular to the molecular plane. The formalism was applied to H_3^+ by Bartlett and Howard,[56] Carter and Meyer,[57,58] and Wolniewicz and Hinze.[59] Alijah, Hinze, and Wolniewicz[60] (AHW) also applied this formalism to H_3^+ using both the MBB and RKJK surfaces.

The calculations using hyperspherical coordinates have been extended to above the barrier to linearity by AHW[60] using the RKJK surface and more recently by Schiffels, Alijah, and Hinze[48,49] (SAH) using the CRJK surface. SAH published their calculations below 9000 cm^{-1} (Part I)[48] and from 9000–13 000 cm^{-1} (Part II)[49] separately. This work is truly *ab initio* since the potential surface is not adjusted to match laboratory data. A comparison by SAH[48] of these theoretical energy values below 9000 cm^{-1} with experimental ones compiled by Lindsay and McCall[14] has revealed a systematic deviation on the order of a fraction of a cm^{-1}, which can be expressed as

$$\Delta E = E_{\text{obs}} - E_{\text{calc}} = -b_1 E_{\text{calc}}^0 - \bar{a}_1 J(J+1) - \bar{a}_2 G^2, \quad (3)$$

where E_{calc}^0 is the calculated band origin and $b_1=1.0123 \times10^{-4}$, $\bar{a}_1=2.0436\times10^{-3}$ cm^{-1}, and $\bar{a}_2=-1.3600 \times10^{-3}$ cm^{-1} are empirical constants. For low rotational levels, the first vibrational term of ΔE is larger than the second and third rotational terms by two orders of magnitude. Since the adiabatic and relativistic corrections are already included in the CRJK potential, SAH[48] ascribe ΔE to the largest of the remaining corrections: that is, the nonadiabatic effect. This leaves the quantum electrodynamic radiative effect as the only remaining sizable correction.

After applying an empirical correction formula similar in form to Eq. (3) but using coefficients based on a least-squares fit to individual experimental band origins, SAH[48] found that approximately 500 laboratory-determined energy levels below 9000 cm^{-1} matched with the calculated levels to within 0.1 cm^{-1}, except for 6 levels whose deviations range from 0.15 to 0.33 cm^{-1}. They also predicted that their

data corrected by the extrapolation formula (3) would have an accuracy of ± 0.1 cm^{-1}. SAH[49] has given predictions for energy levels between 9000 and 13 000 cm^{-1} using this formalism. In the calculations of Watson[36,38] and NMT,[41] who also give energy levels beyond the barrier to linearity, the nonadiabatic and radiative corrections were incorporated empirically when they adjusted the potential surface to fit experimental data.

C. Laboratory spectrum

As evaluated and compiled by Lindsay and McCall,[14] 526 energy levels below 9887 cm^{-1} from vibrational states up to $v_1 + v_2 = 3$ have been experimentally determined: 0 (62), ν_1 (36), ν_2^1 (132), $2\nu_2^0$ (43), $2\nu_2^2$ (116), $\nu_1 + \nu_2^1$ (63), $2\nu_1$ (1), $3\nu_2^1$ (21), $3\nu_2^3$ (14), $\nu_1 + 2\nu_2^0$ (4), $\nu_1 + 2\nu_2^2$ (32), and $2\nu_1 + \nu_2^1$ (2), where the numbers in parentheses give the number of determined rovibrational levels. These data are based on 17 experimental papers which report the fundamental, hot bands, overtone bands, combination bands, and forbidden transitions.

Although overtone and combination bands in ordinary molecules are usually much weaker than the fundamental because their transition dipole moments decrease rapidly for higher vibrational excitation, the decrease in the transition dipole moment of H_3^+ is less drastic than for heavier molecules. Due to the large vibrational amplitude of the protons, the nuclear motion of H_3^+ probes the anharmonic part of the potential surface. We have skipped the third overtone ($4\nu_2^2 \leftarrow 0$) and have searched for the fourth and fifth overtones ($5\nu_2^1 \leftarrow 0$, $6\nu_2^2 \leftarrow 0$) and associated bands. Although these bands are more than 5 times weaker than the third overtone band,[16] these and other associated bands lie in a region where our Ti:sapphire laser has high power and good stability. Since the $5\nu_2^1$ and $6\nu_2^2$ vibrational energy levels are fully above the linearity barrier (Fig. 1), the observed bands are useful for assessing the accuracy of the various theoretical calculations above the barrier to linearity.

III. EXPERIMENT

A liquid-nitrogen-cooled, triple-jacketed discharge tube was used to produce H_3^+.[61] Approximately 500 mTorr of H_2 (and an optional ~ 10 Torr He) was continuously pumped through multiple gas inlets into the central bore (1 m long, 18 mm diameter). The central bore was evacuated by a mechanical pump through multiple outlets, to keep the gas inside the cell fresh. A second jacket filled with liquid nitrogen cooled the inner bore. The outermost jacket was kept sealed under vacuum to provide thermal insulation for the liquid nitrogen. Two CaF$_2$ windows mounted at the appropriate Brewster angle to minimize reflection losses of the laser beam sealed the plasma tube at each end.

A 20 kHz ac potential of 2–5 kV was applied to the electrodes located at each end of the cell, generating a current of up to 1 A. The applied potential was produced by a sine-wave generator amplified by a Techron 7780 power amplifier (4 kW maximum output) and stepped up by a transformer. The maximum H_3^+ signal intensity was obtained with a current of ~ 500 mA rms. These discharge conditions lead

to H_3^+ column densities on the order of 10^{14} cm^{-2}. The resulting plasma is a nonequilibrium system with a rotational temperature of ~ 300 K.

A Coherent 899 titanium:sapphire ring laser pumped by a 10-W Verdi laser provided approximately 1 W of continuous power, high spectral purity (500 kHz bandwidth), and a wide tuning range. The midwavelength optics set was employed in this work, giving continuous coverage from $\sim 11\,000$ to 12 800 cm^{-1}. The laser is computer controlled and can scan over wide regions at lower sensitivity using Coherent's Autoscan software or repetitively over smaller regions (~ 28 GHz) at higher sensitivity using custom software and a National Instruments Data Acquisition (DAQ) Card. Both integration (10 data points per scan step) and coaddition (100 scan segments were averaged for each H_3^+ line) were used to improve the sensitivity. A time constant of 30 ms was used for each scan segment, which was recorded with the sensitivity setting of the lock-in amplifier at 200 μV. Each set of 100 scans took approximately 1 h to record and average.

The combined techniques of velocity modulation[17] and phase modulation[18] were used to improve the sensitivity. This method has been used in the visible region by Longsheng Ma and others at East China Normal University in combination with magnetic rotation for paramagnetic ions[62,63] and in the mid-infrared in this laboratory.[64] Figure 2 shows a schematic of our experimental setup, including the heterodyne detection electronics. We used a New Focus Model 4421 EOM driven by about 2 W of radio frequency power at 500 MHz. High-power, high-transmission Glan laser polarizers from Coherent permitted us to pass approximately 400 mW of laser power through the EOM (limited by the photorefractive damage threshold of the crystal). A 2-GHz étalon spectrum analyzer enabled us to monitor the amplitude of the sidebands; during scanning, we used it to monitor the unmodulated laser beam in order to facilitate calibration of the laser frequency (along with a reference iodine cell heated to $\sim 670\,°$C and a New Focus Model 2011 InGaAs photodetector). Because single-mode lasers such as the Ti:sapphire have little noise at 500 MHz, the beat signals can be detected with a high degree of sensitivity. However, the presence of residual amplitude modulation (RAM) can limit the sensitivity of the technique. Various methods exist for limiting the effect of RAM,[65–69] but the addition of a sample modulation technique such as velocity modulation efficiently eliminates noise and base-line drift caused by RAM.[70,71] A spectral feature that is both velocity-modulated and phase-modulated will appear (approximately) as a second-derivative line shape.

In order to increase the path length of absorption, we used bidirectional optical multipassing. The rf-modulated laser beam was split into two beams with equal intensity by a beam splitter and each beam was passed through the cell cyclically by a set of multiple reflecting mirrors in a modified White cell arrangement so that the effect of the velocity modulation was not canceled. We were able to cleanly obtain four passes through the cell in each direction.

The two beams traveling in opposite directions probed velocity-modulated signals with opposite phases and were
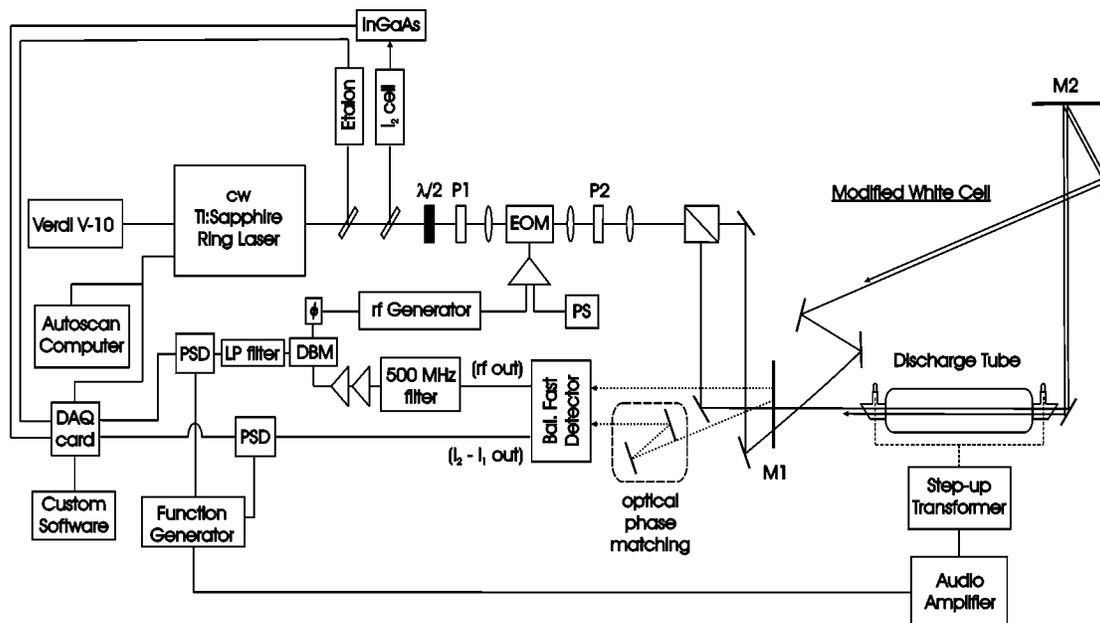
FIG. 2. Experimental setup for the dual-beam, double-modulation technique in the near infrared. The output of the Verdi-pumped Ti:sapphire ring laser ($\sim$400 mW) is split twice and sent into a 2-GHz étalon and through a heated I_2 cell before entering the electro-optic modulator (EOM) and accompanying optics. P1 and P2 are high-power, high-transmission Glan polarizers. A 10-cm lens focuses the laser beam into the center of the EOM, while a second 10-cm lens recollimates the beam. The output of an rf generator is amplified by a high-power rf amplifier (PS=power supply) and is sent to the EOM, which modulates the laser beam at 500 MHz. The modulated laser beam is sent through a 1-m focusing lens and then split into two equal beams with a beam splitter. The two beams travel through the discharge tube in opposite directions 4 times each. M1 and M2 are the two modified White cell multiple reflection optics. After exiting the modified White cell, the two beams are phase matched and optically balanced with neutral density filters.

sent to a set of balanced fast detectors. By balancing the optical power of the two beams with neutral density filters and taking their difference with a New Focus Model 1607-AC fast balanced photoreceiver (650 MHz bandwidth) with two matched silicon photodiodes, the noise was further reduced. The laser noise and noise from the plasma canceled out, and the double-modulated signal approximately doubled in intensity as the path length effectively doubled.

In order to optimize the heterodyne phase in both channels, we used an rf phase shifter (dc-1.0 GHz) from Advanced Technical Materials, Inc. to adjust the overall phase and optically adjusted the phase of the second channel by varying the displacement of a mirror on a track from the second photodiode to match the phases of the two channels. At 500 MHz, an increase or decrease in the path length of the laser beam by $\sim$30 cm results in a phase shift of 180°. Thus by placing a dogleg mirror on a 30-cm track the phase of the second beam can be optimized (with the maximized peak of the second-derivative signal either positive or negative). Because the photoreceiver has three dc outputs (I_1, I_2, and I_1-I_2) in addition to the balanced rf output, we were able to optimize the phase in each detector channel individually so that the subtracted signal (encoded at 500 MHz$\pm$20 kHz) was maximized for phase modulation. The high-frequency output of the detector was sent through a tunable 500 MHz narrow bandpass filter from K & L Microwave, Inc., amplified, and demodulated in a double-balanced mixer referenced to the radio frequency source.

The partially demodulated signal was then sent through a low-pass filter ($<$11 MHz) to a phase-sensitive detector referenced to the sine-wave generator, where the phase of the

velocity modulation was optimized and the signal demodulated at the discharge frequency. The I_1-I_2 dc output of the detector was sent to a second phase-sensitive detector, where it was demodulated at the discharge frequency to give a signal processed by the velocity modulation only. This was particularly helpful when searching for weak lines—although the signal to noise ratio was much worse for the purely velocity-modulated signal, the presence of an apparent first-derivative line shape in the velocity-modulated signal at the same frequency as a second-derivative line shape in the doubly modulated signal helped confirm the presence of a line. Subsequent coaddition helped improve the signal to noise ratio for the transition.

Although the experimental sensitivity is difficult to calculate accurately due to the various components associated with the heterodyne technique, we estimate that our sensitivity limit is close (within an order of magnitude) to the shot-noise limit at our detector, which is $\sim$10^{-8} for a bandwidth of 0.33 Hz and a laser power of $\sim$2 mW impinging on each of the photodiodes. Under these conditions, the best S/N obtained was $\sim$20 (with the coaddition τ=3 s), and the weakest transitions had a S/N of $\sim$3. This suggests that the fractional absorption of the strongest line of H_3^+ is on the order of 10^{-7} and the weakest line has a fractional absorption of $\sim$10^{-8}.

IV. OBSERVED SPECTRUM

Twenty-two H_3^+ transitions to levels above the barrier to linearity and extending into the visible region have been observed, as shown in Table I. Due to the long time needed to

TABLE I. Observed frequencies and assignments.

Assignment	Band	Frequency (cm^{-1})[a]	Rel. int.[b]
$^nR(2,2)^u$	$2\nu_1+2\nu_2^2\leftarrow 0$	11019.358(10)	0.374
$R(1,1)^l$	$5\nu_2^1\leftarrow 0$	11044.149(10)	0.238
$R(3,3)^l$	$5\nu_2^1\leftarrow 0$	11053.680(10)	0.683
$P(3,3)$	$3\nu_1+\nu_2^1\leftarrow 0$	11111.791(10)	0.164
$R(1,0)$	$5\nu_2^1\leftarrow 0$	11228.613(10)	1.000
$R(1,1)^u$	$5\nu_2^1\leftarrow 0$	11244.366(10)	0.258
$R(2,1)^l$	$5\nu_2^1\leftarrow 0$	11246.712(10)	0.131
$R(2,2)^u$	$5\nu_2^1\leftarrow 0$	11304.484(10)	0.191
$Q(1,0)$	$3\nu_1+\nu_2^1\leftarrow 0$	11318.084(10)	0.181
$R(2,1)^u$	$5\nu_2^1\leftarrow 0$	11496.796(10)	0.167
$R(1,0)$	$3\nu_1+\nu_2^1\leftarrow 0$	11503.620(10)	0.123
$^{-6}P(3,3)$	$5\nu_2^5\leftarrow 0$	11571.880(10)	0.165
$R(3,3)^u$	$5\nu_2^1\leftarrow 0$	11576.156(10)	0.276
$^{+6}Q(1,0)$	$5\nu_2^5\leftarrow 0$	11606.160(10)	0.296
$^{+6}R(2,2)$	$5\nu_2^5\leftarrow 0$	11694.790(10)	0.121
$^{+6}R(1,1)$	$5\nu_2^5\leftarrow 0$	11707.265(10)	0.142
$^{+6}R(1,0)$	$5\nu_2^5\leftarrow 0$	11854.463(10)	0.365
$P(2,2)$	$2\nu_1+3\nu_2^1\leftarrow 0$	12222.027(10)	0.119
$^tR(1,0)$	$\nu_1+4\nu_2^2\leftarrow 0$	12246.362(20)	0.121
$P(3,3)$	$2\nu_1+3\nu_2^1\leftarrow 0$	12246.550(20)	0.166
$Q(1,0)$	$2\nu_1+3\nu_2^1\leftarrow 0$	12253.670(10)	0.322
$^tQ(1,0)$	$6\nu_2^2\leftarrow 0$	12419.121(10)	0.227

[a]The uncertainty in the last decimal place is listed in parentheses.
[b]The intensities were calculated at 300 K from the Einstein A coefficients of NMT (Ref. 41).

attain the high sensitivity required to detect these transitions (even the strongest transition could not be detected with a single scan), we did not scan the entire frequency range of the laser ($\sim$1800 cm^{-1}). Instead, we searched for the strongest lines using the intensity information of NMT[41] and the predicted frequencies of both NMT and SAH.[49] Figure 3

shows two examples of spectral lines—the strongest line and a more typical line. As observed in Fig. 3, some of the H_3^+ lines were obscured by the presence of molecular hydrogen Rydberg transitions, which appear as either first- or second-derivative line shapes because some of the Rydberg transitions are velocity-modulated along with the H_3^+ due to electron impact excitation of H_2 into a Rydberg state.[61] These Rydberg lines were often much stronger than the H_3^+ lines, but the addition of 10 Torr of He to the discharge cell (in addition to $\sim$500 mTorr H_2) quenched most of the interfering Rydberg transitions[61] (see the lower trace on the right side of Fig. 3). A notable exception is the very strong Rydberg line at 12 246.425 cm^{-1}. Even with the addition of 20 Torr of He, the Rydberg line did not be disappear completely. The two nearby H_3^+ lines (12 246.362 cm^{-1} and 12 246.550 cm^{-1}) therefore have larger uncertainties than the other H_3^+ lines, because the measurements of their center frequencies (as determined by a second-derivative fitting routine) are affected by the presence of the Rydberg line.

Also listed in Table I are the rotational and vibrational assignments for the observed transitions. These assignments were made based on the intensity information of NMT (which also gives J),[41] the assigned quantum numbers of SAH (which gives vibrational modes, J, G, and rovibrational symmetry),[49,72] and to a lesser extent the calculated expectation values $\langle v_1\rangle$, $\langle v_2\rangle$, $\langle \ell\rangle$, and $\langle G\rangle$ of Watson.[73]

Using the new transition frequencies and the experimentally observed ground state energy levels,[14] experimental upper-state energy levels were determined. Table II shows the assigned approximate quantum numbers from SAH[49,72] and the calculated expectation values of Watson[73] for each of the observed energy levels (expectation values for five of the

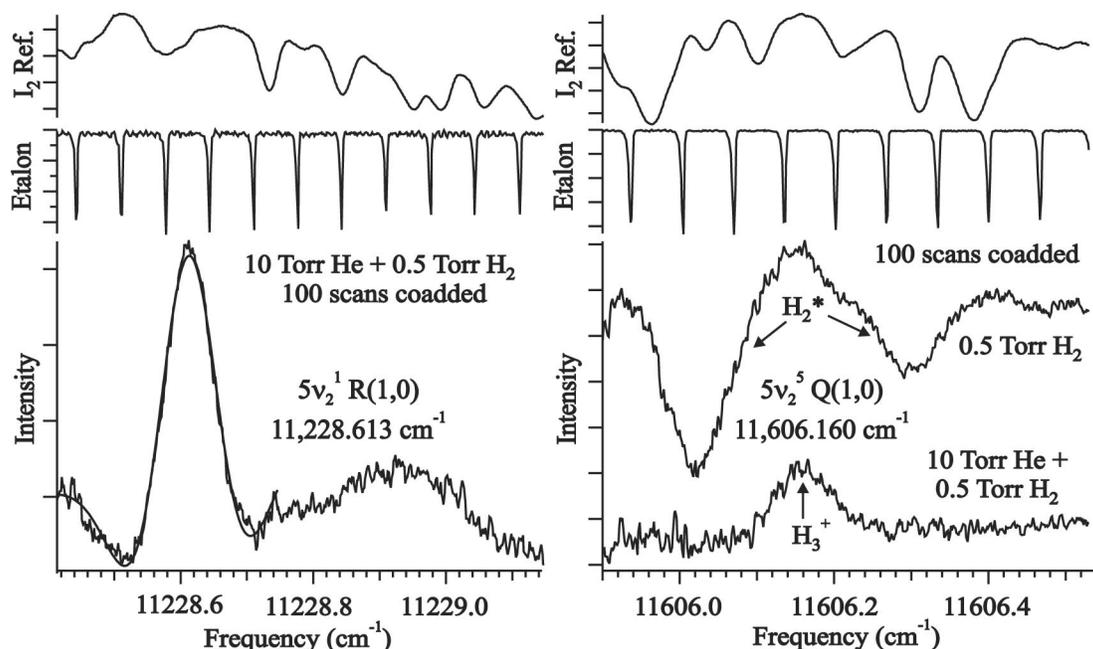
FIG. 3. Strongest observed line (left) and a more typical H_3^+ line buried under two neighboring molecular hydrogen Rydberg lines (right). The addition of 10 Torr of He was usually sufficient to suppress the Rydberg transitions, as shown in the lower right-hand trace. A 2-GHz étalon and a heated I_2 reference cell were used to calibrate the scans after the coaddition. The half width at half maximum (HWHM) for the doubly modulated H_3^+ signal was 1.94 GHz.

TABLE II. Experimentally determined energy levels.

v_1	$\langle v_1 \rangle^a$	v_2	$\langle v_2 \rangle^a$	ℓ	$\langle \ell \rangle^a$	G	$\langle G \rangle^a$	J	n	$\Gamma_{(rv)}$	u/l	Energy (cm^{-1})
0	0.010	5	4.981	1	2.362	1	1.017	2	34	E'	l	11108.270(10)
2	1.390	2	2.909	2	1.560	2	1.658	3	43	E''	u	11188.653(14)
0	0.028	5	4.962	1	1.284	1	1.032	2	35	E'	u	11308.487(10)
0	0.032	5	4.958	1	1.013	0	0.054	2	11	A_2''		11315.573(10)
0	0.051	5	4.912	1	1.206	3	3.178	4	22	A_2'	l	11369.029(14)
3	2.999	1	1.001	1	1.001	0	0.002	1	12	A_2''		11405.044(10)
3	2.990	1	1.012	−1	−1.009	3	2.977	2	14	A_2'		11427.140(14)
0	0.027	5	4.963	1	1.676	2	2.147	3	45	E''	u	11473.779(14)
0	0.025	5	4.964	1	2.084	1	1.035	3	34	E'	l	11484.068(15)
3	2.996	1	1.004	1	1.004	0	0.011	2	12	A_2''		11590.580(10)
0	0.004	5	4.995	−5	−4.983	6	5.980	1	13	A_2''		11693.120(10)
0	---	5	---	1	---	1	---	3	35	E'	u	11734.152(15)
0	0.039	5	4.957	−5	−4.857	5	6.798	2	39	E'		11771.386(10)
0	0.096	5	4.892	−5	−4.576	8	7.365	3	50	E''		11864.085(14)
0	0.044	5	4.953	5	4.565	3	2.884	2	16	A_2'		11887.229(14)
0	0.125	5	4.846	−1	−1.506	3	3.451	4	25	A_2'	u	11891.505(14)
0	0.071	5	4.925	−5	−4.794	6	5.790	2	13	A_2''		11941.423(10)
1	0.958	4	4.040	−2	−2.274	3	3.135	2	14	A_2''		12333.322(20)
2	---	3	---	1	---	0	---	1	15	A_2''		12340.630(10)
2	---	3	---	−1	---	2	---	1	31	E''		12391.322(14)
0	---	6	---	±2	---	3	---	1	16	A_2''		12506.081(10)
2	---	3	---	−1	---	3	---	2	18	A_2'		12561.899(24)

^{a}Expectation values calculated by Watson (Ref. 73); results for five of the energy levels were unavailable. The sign of ℓ could not be determined for the level at 12 506.081 cm^{-1} due to the lack of information about this level.

energy levels were not available). Watson's expectation values agree roughly with the assigned approximate quantum numbers of SAH. Because Watson's expectation values were not available for all of the observed energy levels, the sign of ℓ could not be determined for the level at 12 506.081 cm^{-1}. Also included in Table II are the assigned values of the energy-ordering index n for levels with the same J (starting with $n=1$) and rovibrational permutation inversion symmetry $\Gamma_{(rv)}$.

Figure 4 shows the deviations of the calculated upper-state energy levels from the experimentally observed energy levels. The new experimental H_3^+ lines are compared to the current published theoretical predictions in Table III. The corrected energies by SAH[49] using the CRJK potential energy surface have the best accuracy with an average error of −0.30 cm^{-1} and a standard deviation of 0.31 cm^{-1}; the uncorrected energies have a larger average error (0.845 cm^{-1}) but a slightly smaller standard deviation (0.266 cm^{-1}).
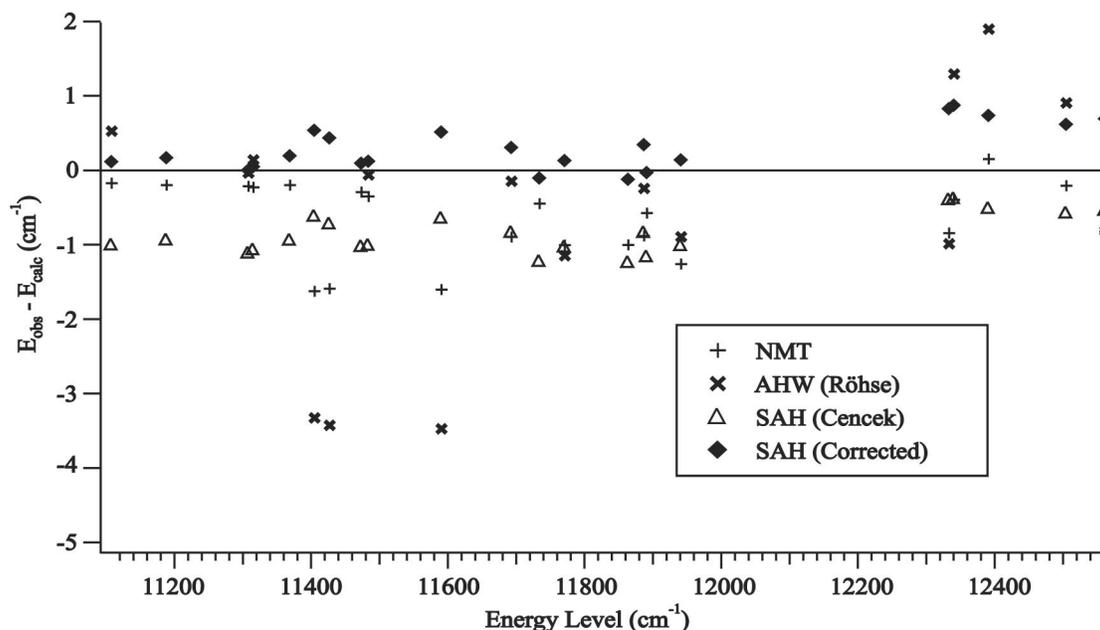

FIG. 4. Observed minus calculated energy levels (see Table III for references). The calculations of SAH (Refs. 49 and 72) most accurately match the experimental data, although their deviation from the observed values seems to increase at higher energies.

TABLE III. Comparison among theoretical and observed transition frequencies.

			Calc.–Obs.		
Band	Observed (cm^{-1})	NMT[a]	AHW[b] (Röhse)	SAH[c] (Cencek)	SAH[c] (corrected)
$2\nu_1 + 2\nu_2^2 \leftarrow 0$	11019.358(10)	0.197	---	0.925	−0.17
$5\nu_2^1 \leftarrow 0$	11044.149(10)	0.172	−0.563	0.998	−0.12
$5\nu_2^1 \leftarrow 0$	11053.680(10)	0.203	---	0.926	−0.19
$3\nu_1 + \nu_2^1 \leftarrow 0$	11111.791(10)	1.594	3.282	0.704	−0.43
$5\nu_2^1 \leftarrow 0$	11228.613(10)	0.230	−0.182	1.062	−0.04
$5\nu_2^1 \leftarrow 0$	11244.366(10)	0.213	−0.001	1.107	−0.01
$5\nu_2^1 \leftarrow 0$	11246.712(10)	0.354	−0.053	0.996	−0.12
$5\nu_2^1 \leftarrow 0$	11304.484(10)	0.290	---	1.011	−0.09
$3\nu_1 + \nu_2^1 \leftarrow 0$	11318.084(10)	1.629	3.286	0.612	−0.53
$5\nu_2^1 \leftarrow 0$	11496.796(10)	0.451	---	1.213	0.10
$3\nu_1 + \nu_2^1 \leftarrow 0$	11503.620(10)	1.604	3.433	0.640	−0.51
$5\nu_2^5 \leftarrow 0$	11571.880(10)	0.885	0.097	0.822	−0.34
$5\nu_2^1 \leftarrow 0$	11576.156(10)	0.577	---	1.148	0.03
$5\nu_2^5 \leftarrow 0$	11606.160(10)	0.897	0.106	0.830	−0.30
$5\nu_2^5 \leftarrow 0$	11694.790(10)	1.001	---	1.225	0.12
$5\nu_2^5 \leftarrow 0$	11707.265(10)	1.007	1.111	1.025	−0.14
$5\nu_2^5 \leftarrow 0$	11854.463(10)	1.262	0.851	1.008	−0.13
$2\nu_1 + 3\nu_2^2 \leftarrow 0$	12222.027(10)	−0.155	−1.983	0.499	−0.74
$\nu_1 + 4\nu_2^2 \leftarrow 0$	12246.362(20)	0.846	0.946	0.390	−0.82
$2\nu_1 + 3\nu_2^1 \leftarrow 0$	12246.550(20)	0.826	0.670	0.523	−0.69
$2\nu_1 + 3\nu_2^1 \leftarrow 0$	12253.670(10)	0.399	−1.335	0.374	−0.87
$6\nu_2^2 \leftarrow 0$	12419.121(10)	0.191	−0.966	0.552	−0.63
	Average error:	0.667	0.544	0.845	−0.30
	Standard deviation:	0.523	1.611	0.266	0.31

[a]Neale, Miller, and Tennyson (Ref. 41).
[b]Alijah, Hinze, and Wolniewicz (Ref. 60).
[c]Schiffels, Alijah, and Hinze (Refs. 49 and 72).

Figure 5 compares the calculated energy levels of SAH[49,72] corrected with the extrapolation formula (3) to all reported energy levels,[14] including this work. The corrected energy levels of SAH become progressively worse with increasing energy. The source of the offsets in the ν_1, $3\nu_2^3$, and $\nu_1 + 2\nu_2^2$ bands can be seen in Fig. 4 of SAH[49]—the band origins for these states are not reproduced well by the correction formula (3). For these bands, a correction formula with coefficients determined from a least-squares fit of the individual experimental band origins is significantly more accurate.[49] The scatter in the errors for the corrected energy levels above the barrier to linearity suggests that none of these band origins are reproduced very accurately by the extrapolation correction formula and that more experimental
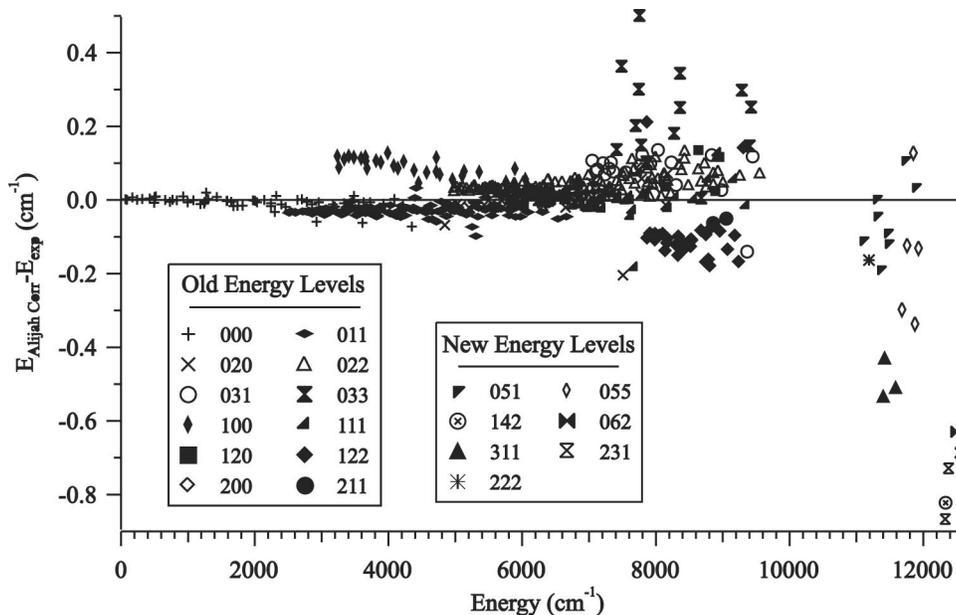

FIG. 5. Comparison between the calculated energy levels of SAH (Refs. 49 and 72) using the extrapolation correction formula [Eq. (3)] and the experimental energy levels reported in Ref. 14 and this work. The scatter in the deviation of the corrected energy levels from the experimental values increases significantly above the barrier to linearity.

band origins are needed to improve the predictive power of Eq. (3).

V. CONCLUSIONS

This work represents a significant step in the spectroscopy of H_3^+. For the first time, transitions to energy levels above the barrier to linearity have been observed. A comparison among current theoretical predictions for these transitions shows most of the calculations to be within 1 cm^{-1} of the experimental energy levels. The average error for even the most accurate of these calculations, however, is still an order of magnitude worse than the most accurate calculations below 9000 cm^{-1}.[14] The availability of experimental data in this region should enable the improvement of theoretical calculations above the barrier.

Although the adiabatic corrections and relativistic corrections for electrons have been theoretically calculated in SAH,[48] the nonadiabatic corrections have yet to be made on H_3^+ from first principles. The rotation-dependent terms of the nonadiabatic corrections in Eq. (3) can be estimated using the relation between the correction to the moment of inertia, $\Delta I_{\alpha\alpha}$, and the rotational g factor $g_{\alpha\alpha}$,

$$\Delta I_{\alpha\alpha} = -\frac{m}{M} g_{\alpha\alpha} I_{\alpha\alpha}, \tag{4}$$

where m and M are the electron mass and proton mass, respectively.[74] The components of the g tensor for H_3^+ theoretically calculated as $g_{aa} = g_{bb} = -0.0686$ and $g_{cc} = -0.0210$ by Oddershede and Sabin[75] and the H_3^+ rotational constants[1] $B = 43.568 \text{ cm}^{-1}$ and $C = 20.708 \text{ cm}^{-1}$ give $\bar{a}_1 = 1.63 \times 10^{-3} \text{ cm}^{-1}$ and $\bar{a}_2 = 2.3 \times 10^{-4} \text{ cm}^{-1}$, compared to SAH's empirical values $2.04 \times 10^{-3} \text{ cm}^{-1}$ and $-1.3 \times 10^{-3} \text{ cm}^{-1}$, respectively. As for nonadiabatic corrections to the vibrational energy, a scaling of the reduced mass based on the theory of Bunker and Moss[76,77] fit the experimental results well, as reported by Polyansky and Tennyson,[45,51] although *ab initio* calculations on the nonadiabatic effect of the kind recently published by Schwenke[78] on H_2O are highly desirable. Such theoretical values will reveal the extent of the radiative correction. Since all these corrections are larger for higher energies, experimental values presented in this paper will give a crucial test of the theory.

With continuing improvements in sensitivity (such as more coaddition) this work can be extended to higher overtone bands of H_3^+ ($6\nu_2^4 \leftarrow 0$, $7\nu_2 \leftarrow 0$, etc.), continuing the climb up the energy ladder of H_3^+ and further testing theoretical predictions and potentials. The lack of assigned spectroscopic data in the energy regime from 10 000 to 35 000 cm^{-1} (until this work) means that the potential is not strongly constrained.[79] Consequently, none of the potential energy surfaces near the H_3^+ dissociation limit ($\sim 35\,000 \text{ cm}^{-1}$) are considered reliable, and experimental data on higher-energy levels are needed to improve them. An improved potential energy surface might finally enable the analysis of the near-dissociation spectrum, which has remained completely unassigned since its discovery by Carrington *et al.*[80] 20 years ago.

[1] T. Oka, Phys. Rev. Lett. **45**, 531 (1980).
[2] L. Trafton, D. F. Lester, and K. L. Thompson, Astrophys. J. Lett. **343**, L73 (1989).
[3] P. Drossart, J. P. Maillard, J. Caldwell *et al.*, Nature (London) **340**, 539 (1989).
[4] T. R. Geballe and T. Oka, Nature (London) **384**, 334 (1996).
[5] B. J. McCall, T. R. Geballe, K. H. Hinkle, and T. Oka, Science **279**, 1910 (1998).
[6] T. Oka, in *Molecular Ions: Spectroscopy, Structure, and Chemistry*, edited by T. A. Miller and V. E. Bondybey (North-Holland, Amsterdam, 1983), p. 73.
[7] T. Oka, Rev. Mod. Phys. **64**, 1141 (1992).
[8] S. Miller and J. Tennyson, Chem. Soc. Rev. **21**, 281 (1992).
[9] J. Tennyson and S. Miller, Contemp. Phys. **35**, 105 (1994).
[10] A. Dalgarno, Adv. At., Mol., Opt. Phys. **32**, 57 (1994).
[11] I. R. McNab, Adv. Chem. Phys. **89**, 1 (1995).
[12] J. Tennyson, Rep. Prog. Phys. **57**, 421 (1995).
[13] B. J. McCall, Philos. Trans. R. Soc. London, Ser. A **358**, 2385 (2000).
[14] C. M. Lindsay and B. J. McCall, J. Mol. Spectrosc. **210**, 60 (2001).
[15] J. Tennyson and S. Miller, Spectrochim. Acta, Part A **57**, 661 (2001).
[16] B. J. McCall, Ph.D. thesis, University of Chicago, 2001, available online at http://fermi.uchicago.edu/publications/archive/mccallthesis.pdf
[17] C. S. Gudeman, M. H. Begemann, J. Pfaff, and R. J. Saykally, Phys. Rev. Lett. **50**, 727 (1983).
[18] G. C. Bjorklund, Opt. Lett. **5**, 15 (1980).
[19] J. P. Maillard and E. Lellouch (private communication).
[20] T. Oka, J. Mol. Spectrosc. **48**, 503 (1973).
[21] J. T. Hougen, J. Chem. Phys. **37**, 1433 (1962).
[22] J. B. Anderson, J. Chem. Phys. **96**, 3702 (1992).
[23] C. A. Coulson, Proc. Cambridge Philos. Soc. **31**, 244 (1935).
[24] G. D. Carney and R. N. Porter, J. Chem. Phys. **60**, 4251 (1974).
[25] G. D. Carney and R. N. Porter, J. Chem. Phys. **65**, 3547 (1976).
[26] W. Meyer, P. Botschwina, and P. Burton, J. Chem. Phys. **84**, 891 (1986).
[27] S. Miller and J. Tennyson, J. Mol. Spectrosc. **126**, 183 (1987).
[28] S. Miller and J. Tennyson, J. Mol. Spectrosc. **128**, 530 (1988).
[29] S. Miller and J. Tennyson, J. Mol. Spectrosc. **136**, 223 (1989).
[30] B. T. Sutcliffe and J. Tennyson, J. Chem. Soc., Faraday Trans. 2 **83**, 1663 (1987).
[31] M. G. Bawendi, B. D. Rehfuss, and T. Oka, J. Chem. Phys. **93**, 6200 (1990).
[32] W. A. Majewski, P. A. Feldman, J. K. G. Watson, S. Miller, and J. Tennyson, Astrophys. J. Lett. **347**, L51 (1989).
[33] L.-W. Xu, M. Rösslein, C. M. Gabrys, and T. Oka, J. Mol. Spectrosc. **153**, 726 (1992).
[34] B. M. Dinelli, S. Miller, and J. Tennyson, J. Mol. Spectrosc. **163**, 71 (1994).
[35] G. C. Lie and D. Frye, J. Chem. Phys. **96**, 6784 (1992).
[36] J. K. G. Watson, Can. J. Phys. **72**, 702 (1994).
[37] J. K. G. Watson, Chem. Phys. **190**, 291 (1995).
[38] J. K. G. Watson (private communication).
[39] R. Röhse, W. Kutzelnigg, R. Jaquet, and W. Klopper, J. Chem. Phys. **101**, 2231 (1994).
[40] B. M. Dinelli, O. L. Polyansky, and J. Tennyson, J. Chem. Phys. **103**, 10433 (1995).
[41] L. Neale, S. Miller, and J. Tennyson, Astrophys. J. **464**, 516 (1996).
[42] B. M. Dinelli, C. R. Le Sueur, J. Tennyson, and R. D. Amos, Chem. Phys. Lett. **232**, 295 (1995).

J. Chem. Phys., Vol. 118, No. 24, 22 June 2003

Near-infrared spectroscopy of H_3^+ 10899

[43] W. Cencek, J. Rychlewski, R. Jaquet, and W. Kutzelnigg, J. Chem. Phys. **108**, 2831 (1998).

[44] R. Jaquet, W. Cencek, W. Kutzelnigg, and J. Rychlewski, J. Chem. Phys. **108**, 2837 (1998).

[45] O. L. Polyansky and J. Tennyson, J. Chem. Phys. **110**, 5056 (1999).

[46] R. Jaquet, Chem. Phys. Lett. **302**, 27 (1999).

[47] R. Jaquet, Spectrochim. Acta, Part A **58**, 691 (2002).

[48] P. Schiffels, A. Alijah, and J. Hinze, Mol. Phys. **101**, 175 (2003).

[49] P. Schiffels, A. Alijah, and J. Hinze, Mol. Phys. **101**, 189 (2003).

[50] A. Aguado, O. Roncero, C. Tablero, C. Sanz, and M. Paniagua, J. Chem. Phys. **112**, 1240 (2000).

[51] M. A. Kostin, O. L. Polyansky, and J. Tennyson, J. Chem. Phys. **116**, 7564 (2002).

[52] R. M. Whitnell and J. C. Light, J. Chem. Phys. **90**, 1774 (1989).

[53] B. R. Johnson, J. Chem. Phys. **79**, 1916 (1983).

[54] F. T. Smith, J. Math. Phys. **3**, 735 (1962).

[55] R. C. Whitten and F. T. Smith, J. Math. Phys. **9**, 1103 (1968).

[56] P. Bartlett and B. J. Howard, Mol. Phys. **70**, 1001 (1990).

[57] S. Carter and W. Meyer, J. Chem. Phys. **93**, 8902 (1990).

[58] S. Carter and W. Meyer, J. Chem. Phys. **100**, 2104 (1994).

[59] L. Wolniewicz and J. Hinze, J. Chem. Phys. **101**, 9817 (1994).

[60] A. Alijah, J. Hinze, and L. Wolniewicz, Ber. Bunsenges. Phys. Chem. **99**, 251 (1995).

[61] B. J. McCall and T. Oka, J. Chem. Phys. **113**, 3104 (2000).

[62] R. Wang, Y. Chen, P. Cai, J. Lu, Z. Bi, X. Yang, and L. Ma, Chem. Phys. Lett. **307**, 339 (1999).

[63] M. Luo, Z. Bi, P. Cai, R. Wang, X. Yang, Y. Chen, and L. Ma, Rev. Sci. Instrum. **72**, 2691 (2001).

[64] C. M. Lindsay, Ph.D. thesis, University of Chicago, 2002, available online at http://fermi.uchicago.edu/publications/archive/lindsaythesis.pdf

[65] M. Gehrtz, G. C. Bjorklund, and E. A. Whittaker, J. Opt. Soc. Am. B **2**, 1510 (1985).

[66] G. C. Bjorklund, M. D. Levenson, W. Lenth, and C. Ortiz, Appl. Phys. B: Photophys. Laser Chem. **32**, 145 (1983).

[67] N. C. Wong and J. L. Hall, J. Opt. Soc. Am. B **2**, 1527 (1985).

[68] J. A. Silver and A. C. Stanton, Appl. Opt. **27**, 1914 (1988).

[69] E. A. Whittaker, C. M. Shum, H. Grebel, and H. Lotem, J. Opt. Soc. Am. B **5**, 1253 (1988).

[70] J. L. Hall, L. Hollberg, T. Baer, and H. G. Robinson, Appl. Phys. Lett. **39**, 680 (1981).

[71] W. E. Sinclair, D. Pfluger, H. Linnartz, and J. P. Maier, J. Chem. Phys. **110**, 296 (1999).

[72] A. Alijah (private communication).

[73] J. K. G. Watson (private communication).

[74] T. Oka and Y. Morino, J. Mol. Spectrosc. **6**, 472 (1961).

[75] J. Oddershede and J. R. Sabin, Chem. Phys. **122**, 291 (1988).

[76] P. R. Bunker and R. E. Moss, Mol. Phys. **33**, 417 (1977).

[77] P. R. Bunker and R. E. Moss, J. Mol. Spectrosc. **80**, 217 (1980).

[78] D. W. Schwenke, J. Phys. Chem. A **105**, 2352 (2001).

[79] J. Tennyson, M. A. Kostin, H. Y. Mussa, O. L. Polyansky, and R. Prosmiti, Philos. Trans. R. Soc. London, Ser. A **358**, 2419 (2000).

[80] A. Carrington, J. Buttenshaw, and R. Kennedy, Mol. Phys. **45**, 753 (1982).